Impact Flows and Loads on Ship-Deck Structures

M. Greco and M. Landrini
INSEAN
The Italian Ship Model Basin
Via di Vallerano 139
00128 Roma, Italy

O.M. Faltinsen
Department of Marine Hydrodynamics
NTNU
Otto Nielsens rd. 10
N-7491 Trondheim, Norway

Abstract

The shipping of water on the deck of a vessel in head-sea conditions and zero-forward speed is investigated by experimental and numerical means. The main stages of the fluid-dynamic phenomenon are identified and the related structural loading conditions are studied. It is shown that potential-flow modeling suffices to give a robust estimate of green-water loads until large breaking phenomena, usually following impact events, are observed.

Introduction

The practical prediction of wave-induced ship motions and loads has reached a reliable degree of maturity since the 70's, when the strip-theory codes became available, Salvesen *et al.* (1970). The need to estimate occurrence and severity of dangerous events, such as the shipping of water on the deck of vessels, is not of minor importance but rational prediction tools are not yet available. A fuller understanding of the fluid dynamics involved in, and the ability to predict and control water-shipping events are the general goals of an ongoing research activity, Greco *et al.* (2000a) - Greco *et al.* (2002b), which will be partly recalled in the following.

Here, we consider a synergic investigation where experimental studies are combined with numerical modeling to identify the relevant parameters and to define possible simplified approaches of practical value. In particular, we focus our attention on the structural consequences of the water invading and flowing along the deck, and finally impacting against the deck house in the bow region of a Floating Production Storage and Offloading ship (FPSO) with zero forward speed in head-sea conditions.

FPSO units represent a relatively new concept of oil platform, where a ship moored in open sea is used for production, storage and offloading operations. Generally, FPSOs are cheap to build. However, the lower price is balanced by narrower limits of operation conditions because of the larger motion amplitudes with respect to those of other platforms types. Further, the construction of dedicated equipment (for instance the turret) can be expensive. Unlike semi-submersible and TLP structures, an important feature of FPSOs is represented by the possibility of providing storage capacity for the crude oil. Further, FPSOs can work in a wide range of water depths, and have a larger deck space for operation and equipment. Finally, in hurricane or iceberg areas FPSOs can disconnect and move away from the danger. On the downside, FPSOs can suffer relatively large vessel motions, since natural periods in heave, pitch and roll lie within the wave frequency range. FPSOs are supposed to be weather-vaning, that is head-sea condition is the most-occurring operation condition, and water on deck in the bow region is considered an important risk be taken into account to define operational strategies and ship design. Green-water accidents documented both deck wetness in the bow region and from the ship sides, with damages for deck house and equipment. The location of the deck house can vary: usually FPSOs working in the North Sea have the deck house in the bow region, while units operating in South America have the deck house near the stern.

In this paper, a first global understanding of the phenomenon is gained through experimental investigations. In particular, these allow for identifying the main stages of the flow-field evolution. Each of these is of concern from a structural point of view, and will be further investigated in the second part of the paper. Upon assuming realistic parameters for the ship structure, we define the criticality of the different flow stages and the reliability of the

Paper presented at the RTO AVT Symposium on "Reduction of Military Vehicle Acquisition Time and Cost through Advanced Modelling and Virtual Simulation", held in Paris, France, 22-25 April 2002, and published in RTO-MP-089.

mathematical model to deal with. Finally, the role of hydroelasticity in deck-house impacts after water shipping is addressed.

Experimental investigation of water shipping

Three-dimensional model experiments

Three-dimensional experiments have been performed to study water-on-deck phenomena on the Esso-Osaka tanker, restrained to move, in head-sea conditions and without forward speed. The model has draft D=0.284m, length between the perpendiculars L=4.44m and beam B=0.74m. The tests have been carried out at INSEAN facilities, in the Towing Tank 2 (length 220m, breadth 9m and depth 3.6 m). By considering FPSO ships and their usual operation conditions, we have determined the main incident wave parameters. In particular, the FPSO water-on-deck accidents in the North Sea documented that the most interesting wavelengths are of the order of the ship length. Further, several casualties occurred during full-loaded conditions, when the effective freeboard is smaller than the nominal value, see Ersdal and Kvitrud (2000). To have realistic heights of water relative to the deck for representative design conditions, the upper portion of the bow has been modified by reducing the freeboard to f=0.064 m, resulting in the non-dimensional parameters $D/L\approx0.064$, $B/L\approx0.166$ and $f/L\approx0.015$.

The analysis has been carried out by combining flow visualizations, image analysis and wave elevation measurements around the bow region. In particular, the uppermost portion of the hull and the bow region of the deck have been made by transparent material to permit visualizations of the water running up along the bow, entering the deck and flowing against a vertical Plexiglas plate to mimic a deck-house wall. To the purpose, a video camera has been used in combination with a mirror placed under the ship deck. The flow evolution was recorded through a black/white video camera with a frame rate of 30Hz.

In real cases, water shipping may be due either to a single large wave, or to the cumulative effect of a small number of events associated with wave groups approaching the ship. In the latter case, the first event is not necessarily the most severe one. In the present tests, the water on deck is caused by a single event due to a wave packet. In this way, we also avoid effects due to wave reflections from the tank walls. The incident wave packet results from the focusing of several wave components generated with suitable phase relationship, Rapp and Melville (1990). The wave spectrum and the focusing point along the tank represent the input data. In the present case, each component has the same amplitude a. A characteristic steepness $k_c a$ of the wave packet can be defined by the wavenumber k_c associated with the mean frequency f_c of the spectrum. In tests here reported, we have chosen f_c=0.6 Hz and the frequency bandwidth Δf=0.4Hz, respectively. This gives a characteristic wavelength $\lambda_c=2\pi k_c=4.33\text{m}\approx0.98L$. The shortest and the longest wave components correspond to about $0.5L$ and to about $2.6L$, respectively. The wave steepness $k_c a$ has been varied between 0.125 and 0.25. A fuller presentation and an in-depth discussion of the experimental results is reported in Greco *et al.* (2002b), here we summarize the main physical findings.

The sequence of pictures in Fig.1 shows the interaction of the wave packet approaching the ship bow from left to right. After the water exceeds the freeboard, it enters the deck in a non-uniform manner because of the three-dimensionality of the hull form. At the beginning, the water plunges onto the deck at the fore portion of the bow, as indicated by the white arrows in the pictures. As time passes, the shipped water starts to flow along the deck, while the freeboard is exceeded along the ship sides. Later on, the water impacts against the vertical wall in a complex fashion, starting from the lateral sides.

The bottom view in Fig.2 highlights the formation of air entrapment during the early stages of the water shipping. In particular, the right picture shows two cavities developing along the bow edges, with varying cross section and maximum area near the ship centerline.

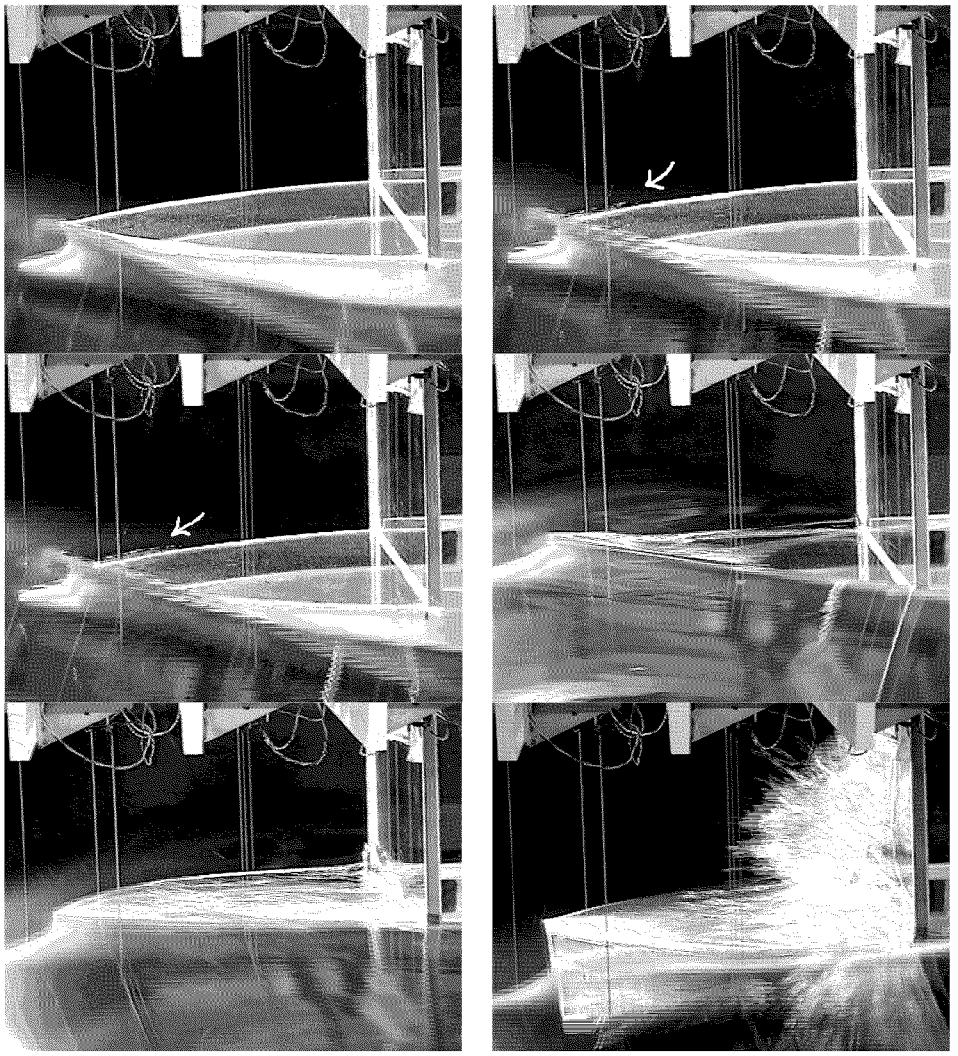

Figure 1. Side view of the water shipping on an ESSO-Osaka model induced by a wave packet, propagating from left to right. The white arrows indicate the region where the water front plunges onto the deck. Time increases from left to right and from top to bottom. The two bottom pictures show the interaction with the vertical wall.

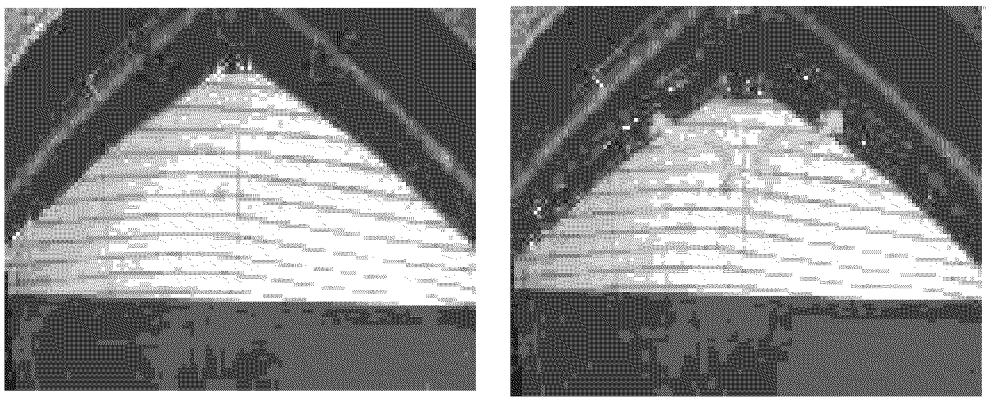

Figure 2. Initial stages of the water shipping. Left: the red arrows show the direction of the water flow entering the deck. Right: the green arrows indicate the location of the cavity structures along the bow sides.

A more complete analysis of the taken flow visualizations led to the interpretation of the fluid-flow evolution during the initial stage of the water shipping, as explained in Fig.3. When the water exceeds the freeboard, the fluid front plunges onto the deck, forming the already mentioned air cavity (sketch 1). As the wave packet propagates downstream the hull, "fresh" water enters the deck along the bow sides, and moves initially inwards. Because of the symmetry of the phenomenon, the lateral water fronts approach each other in proximity of the ship centerline and are diverted outwards by the mutual interaction (sketch 2). An inner blunt fluid structure results from this interaction. As time passes, this structure is fed by the water shipped laterally and moves along the deck towards the deck house (sketch 3). The fourth sketch shows the structure of the water front before the impact against the vertical wall. It is worth stressing the non-uniform distribution of water height, with a maximum value occurring around the ship centerline.

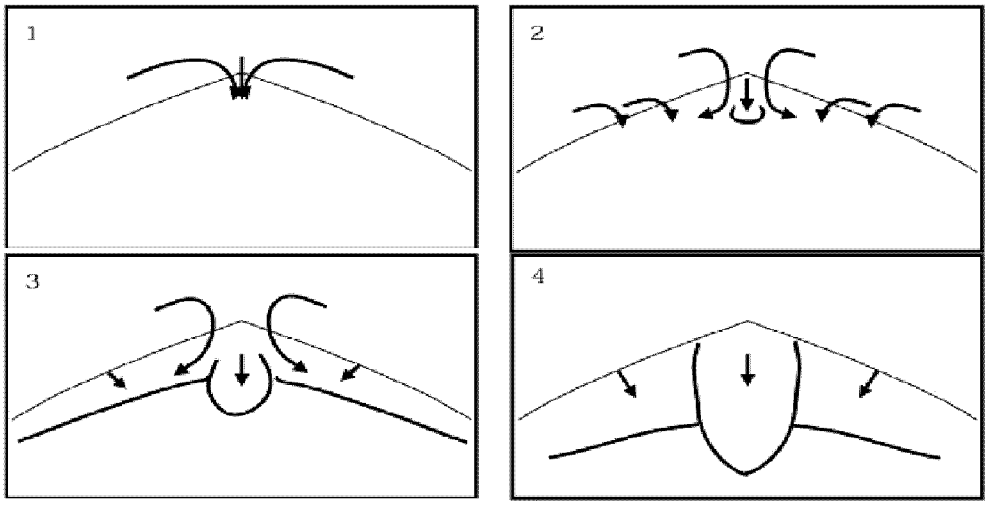

Figure 3. Interpretation of the fluid-flow evolution during the initial stage of the water shipping. 1: The water exceeds the freeboard and plunges onto the deck; 2: The fluid flowing from the lateral sides is diverted outwards along the centerline, and a central blunt water front appears; 3: Intensification of the fluid motion transverse to the dam break-type front and growth of the inner water tongue propagating along the ship centerline; 4: Gross structure of the water front before the impact against the vertical wall.

Two-dimensional laboratory tests

For a clearer understanding of the water shipping dynamics, and to guide the developing of numerical methods, two-dimensional water-on-deck laboratory tests have been performed in the narrow wave flume (length 13 m, depth 1 m and width 0.6 m) at the Department of Marine Hydrodynamics of NTNU. Incoming waves are generated by a flap wavemaker. The body-parameters here considered are: draft D = 0.2 m, length L = 1.5 m, freeboard f = 0.05 m. The bottom corner at the model was rounded with a radius of curvature 0.08 m to avoid significant vortex shedding. Body motions are restrained. Since the generated wave system is highly transient, with the first crest generally steeper than the following ones, we decided to focus our study on the first water-shipping event.

The fundamental stages of the water shipping and the interaction with the deck first, and later with the superstructure are described through the pictures in Figs. 4-6. In particular, Fig. 4 reports the enlarged view of the water front entering the deck. The shipping of the fluid initiates with water plunging directly onto the deck, *cf.* the top-left frame. At this stage, high impact pressures are expected. However, the very high pressures last too short and are too concentrated in space to be dangerous for the structure. After the impact, a cavity entrapping air is formed, as shown in the top-right and following frames. The changes of the cavity volume due to the motion of the surrounding fluid determine time-varying loads on the deck. This phase of the fluid-structure interaction may damage the deck at least if the air in the cavity cannot escape. The latter occurs more easily in three- dimensional conditions rather than in the two-dimensional flow field here considered.

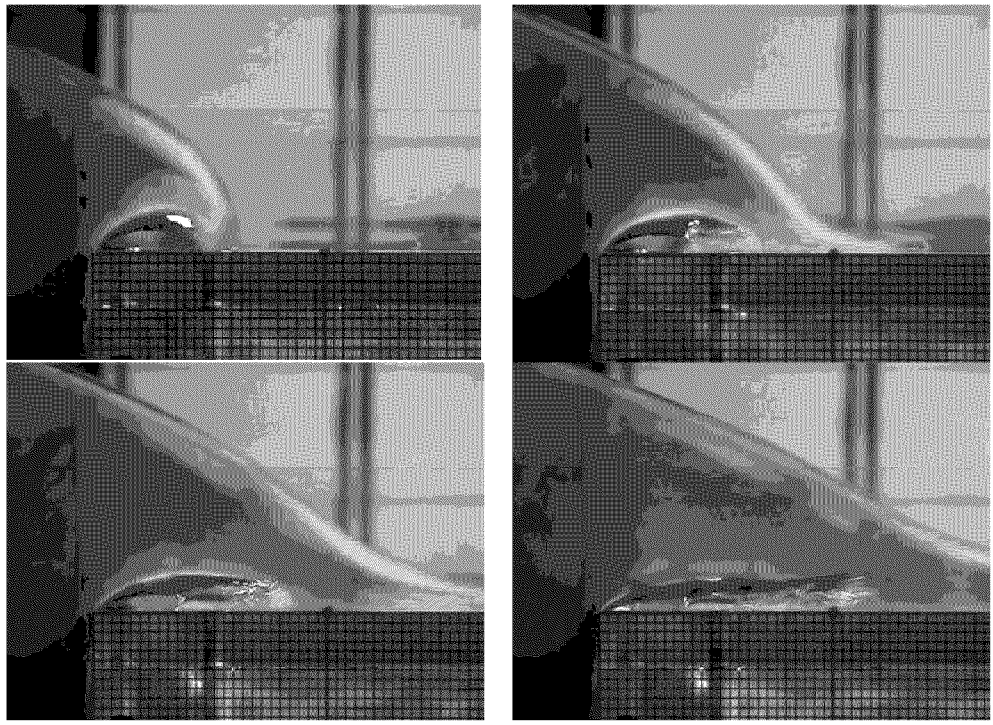

Figure 4. Initial stages of the water shipping: the water front plunges onto the deck forming an air pocket, which is squeezed and stretched downstream by the main flow. Time increases from left to right and from top to bottom.

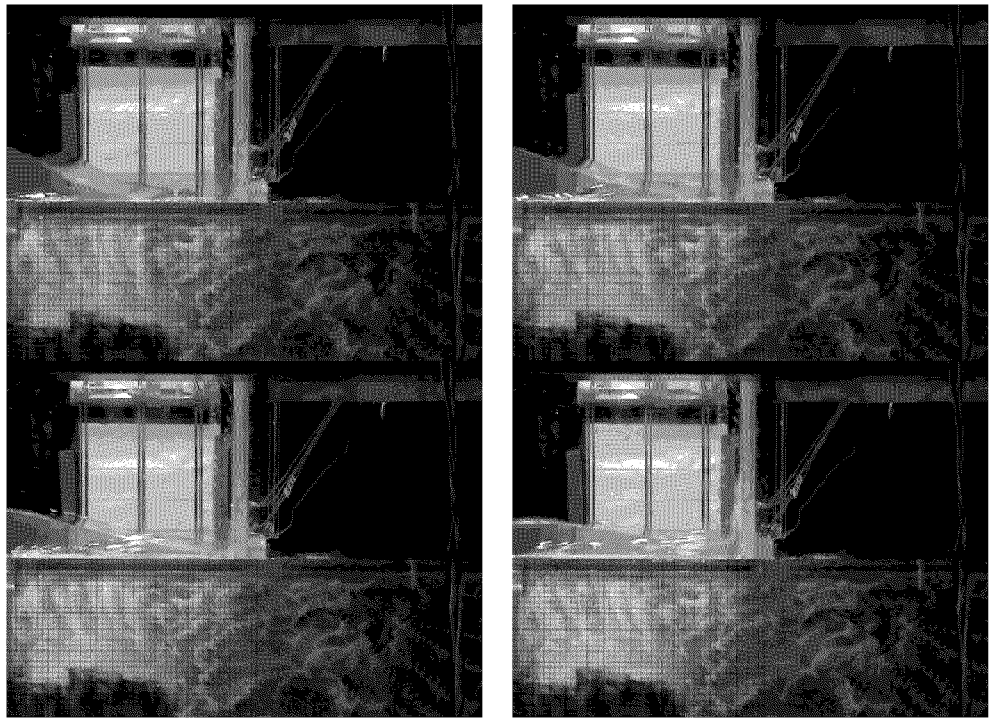

Figure 5. Dam break-type flow developing along the deck and eventually hitting the vertical superstructure. Time increases from left to right and from top to bottom.

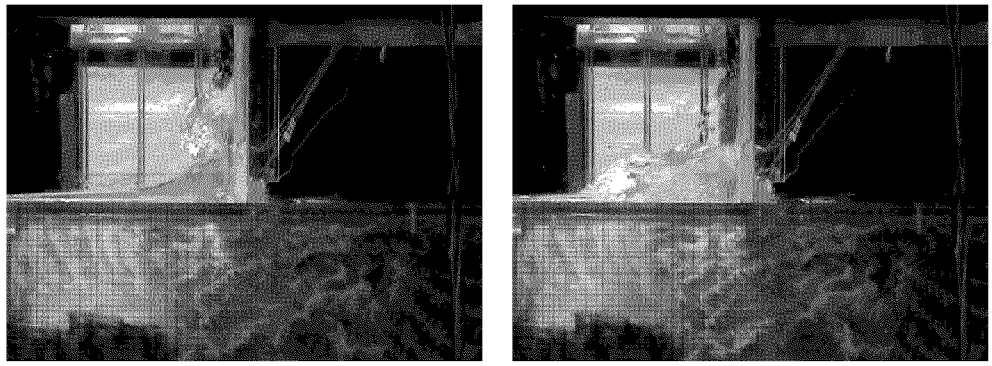

Figure 6. Late evolution of the impact against the vertical superstructure: after the maximum run-up the water plunges backwards onto the deck.

After a time short with respect to the duration of the entire water-shipping, the gross features of the flow field resemble those originated after the breaking of a dam, as shown in Fig. 5. Namely, a tongue of fluid develops along the deck, without observation of free-surface breaking. Therefore, the gross fluid dynamics is rather simple, with practically hydrostatic loads in proximity of the water front. In this context, an additional important contribution to local loads would be given by ship motions, though not allowed in our experiments. Actually, numerical results show that there are important interactions between the flow on the deck and the flow field exterior to the vessel. This limits the similarity with dam-break flows and the practical possibility of using shallow-water models (see Greco *et al.* (2000c)).

Finally, the impact against the vertical structure is observed (bottom frames in Fig. 5). In the following evolution, *cf.* Fig. 6, the fluid rises rapidly along the vertical wall. The fluid run up is slowed down by the action of the gravity, and the water front thickens. After the maximum run up has been reached, the water collapses downwards, and a backward overturning is observed.

Analysis of the fluid-structure interaction

In the following, the structural implications of the fluid-structure interaction associated with the shipping of water are investigated. To the purpose, both numerical and experimental data will be used in a combined fashion. According to the previous discussion, three different stages of the water shipping will be considered.

Initial plunging phase and deck impact The first three plots of Fig. 7 show the initial plunging phase observed in the two-dimensional experimental investigation, and the comparison with the numerical prediction obtained by a potential-flow model. The statement of the mathematical problem and the details of the Boundary Element Method developed for its solution are discussed in Greco *et al.* (2000b). In the figure, the waves (λ/D = 10.1, H/D = 0.808) approach the obstacle from left to right and the numerical results are in rather good agreement with the experimental visualization. In the simulation, surface-tension effects have not been modeled, which suggests a limited role of surface tension in determining the initial volume of the entrapped cavity, at least for the wave parameters here considered. Upon this validation, we can use the numerical tool to investigate in more detail the local features of the phenomenon. In the right plot of the same figure, the numerical free-surface configuration (solid line) at the impact is given. It is also shown that close to the separation point at the bow, the cavity profile is well fitted by the local solution $z_1 = C(t)x_1^{2/3}$ (line with circles, *cf.* Zhao *et al.* (1997)) around the fixed separation point. This approximation is obtained by assuming a potential flow and neglecting the gravity effects. In this local solution, the origin of the local coordinate system (x_1,z_1) is at the edge of the deck, the x_1-axis is along the deck and the z_1 axis is vertically upwards. The coefficient $C(t)$ is a time dependent parameter which depends on the complete flow, and therefore cannot be determined by a local flow analysis. The part of the water front impacting on the deck agrees well with a parabolic contour (line with black squares), which would be the path of a free-falling fluid particle. Therefore, at the beginning of the water shipping, the fluid undergoes three stages of evolution: (i) the fluid is diverted vertically upwards, with negligible effects of the gravity; (ii)

an intermediate phase with almost horizontal motion where gravity and pressure gradients are comparable, and (iii) a free-falling evolution up to the impact point.

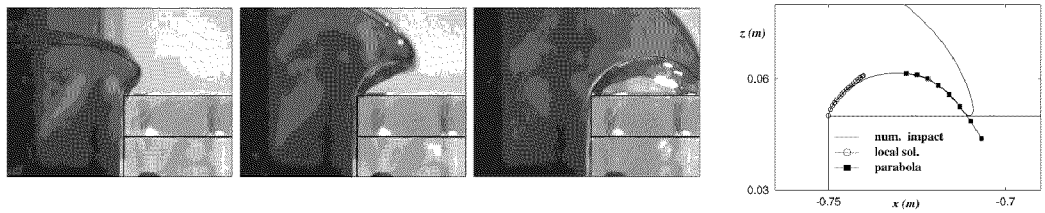

Figure 7. Initial stages of water shipping. Left: the numerical results (red lines) are compared with the experiments. Time increases from left to right. Right: the numerical solution (solid line) is compared with a local solution (line with circles) and with a free-fall trajectory (line with squares).

From a structural perspective, the plunging phase is characterized by the water impact against the deck and the air-cushion phenomenon. In the following, the related effects on the deck of a real FPSO unit have been investigated. In the considered ship, the steel stiffeners along the deck are sketched in the left diagram of Fig. 8. The deck is designed to stand against a maximum spatially uniform pressure of 60 KPa and has been modeled as an equivalent beam (*cf.* the left sketch in Fig. 8) along a longitudinal stiffener.

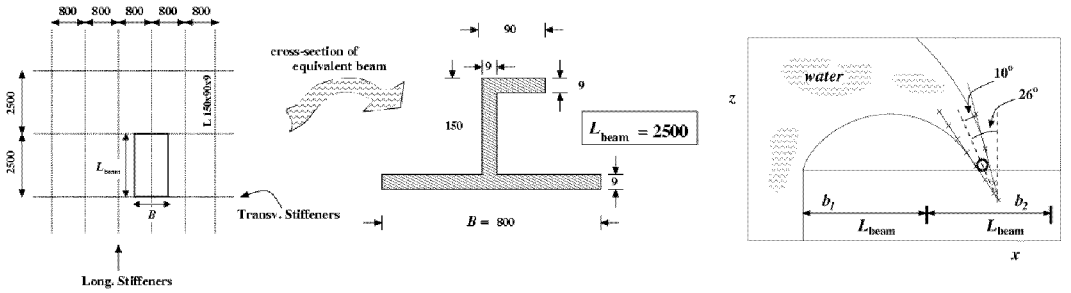

Figure 8. Left: example of stiffeners on the deck of a FPSO, top view and cross-section of the equivalent beam to model the deck in the longitudinal direction. Dimensions are in millimeters. Right: numerical solution at the impact. Close to the impact position, the free surface (solid line) is approximated by a circle with radius $r \approx 0.1$ m. The free surface resembles a fluid wedge of about 20°, inclined of approximately 26° with respect to the vertical direction. The two horizontal arrows (b_1 and b_2) indicate the length of the first and second equivalent beams along the deck.

At full scale, we consider the water impact following the shipping of water caused by incident waves with length 182 m, and height 14.55 m (corresponding to the wave parameters mentioned above, with the FPSO draft equal to 18 m). The free-surface configuration as obtained by the numerical simulation is given in the right plot of Fig. 8. The two horizontal arrows indicate the length of the first two equivalent beams along the deck. The impact starts close to the middle of the second one. From the numerical simulation, an impact velocity of 4.3 m/s is estimated. This value is not large, and in particular is close to the orbital velocity in free-wave conditions (4.4 m/s). The free-surface shape near the initial impact position is rather blunt, with radius of curvature $r \approx 0.1$ m.

The portion of flow field on the deck and closer to the bow is characterized by the cavity originated at the impact instant. During the evolution, the air cavity is stretched by the flow entering the deck and above it. As a consequence, the beam b_1, initially under the action of the atmospheric pressure, suffers loads due to the compressibility of the air entrapped in the cavity. If we assume a uniform pressure in the cavity, and we model the air evolution as an adiabatic process of an ideal gas, the pressure $p(t)$ in the cavity can be obtained by $p(t)/p_0 = \left(V(t)/V_0\right)^{\gamma}$. Here, $p(t)$ and $V(t)$ are the pressure and the volume at time t and p_0 and V_0 are the corresponding reference values, *e.g.* the atmospheric pressure (p_0=1 Atm $\approx 10^5$ Pa) and the air volume in the cavity at the impact instant. The usual value $\gamma = 1.4$ is used for the ratio of the specific heats.

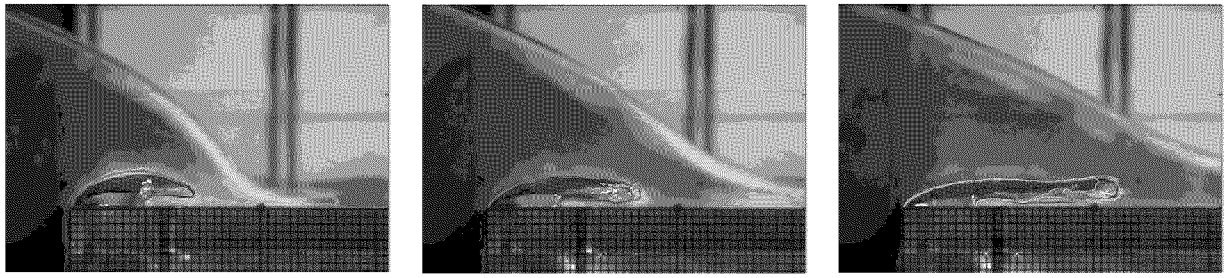

Figure 9. Evolution of the air cavity at the bow edge. The time increases from left to right with a constant interval of 0.38 s (at full scale, D = 18 m). The digitized cavity profiles (colored lines) are superimposed to the video images.

By using the above model and the pictures taken from the experiments, we have carried out a simplified analysis to evaluate the pressure acting on the first beam. In the sequence of Fig. 9, the post-impact evolution is shown with snapshots separated in time by an interval of 0.38 s. Because of the relatively poor resolution of the images, at least for the present purpose, the cavity profile is not sharply detectable from the pictures, and for each snapshot several different curves are candidates as cavity boundary. Therefore, all of them have been considered and are reported, superimposed to the corresponding video images. For each instant of time, the cavity volume has been evaluated and used to estimate the pressure inside the cavity. Because of the uncertainty in the determination of the cavity boundary, for each time step several scattered results will be obtained. Actually, even this simplified analysis requires some extra data, which have been deduced from the numerical simulations. In particular, the cavity volume V_0 at the impact instant t_{imp} is computed numerically. The circles in the left plot of Fig. 10 represent the pressure computed according to the above procedure. As anticipated, different pressure values at the same time instant are obtained, corresponding to different digitized cavity boundaries. The pressure envelope (dashed lines) gives an indication of the order of magnitude of the uncertainty involved in. In the plot, the horizontal solid line is the design pressure for the deck. According to the present analysis, this value can be exceeded during the cavity evolution, and likely this occurs for a time interval not small compared with the first natural dry-beam period $T_{\text{dry 1}}$. Therefore, the collapse of the cavity can be critical for the strength of the deck structure and hydroelastic effects may be also relevant.

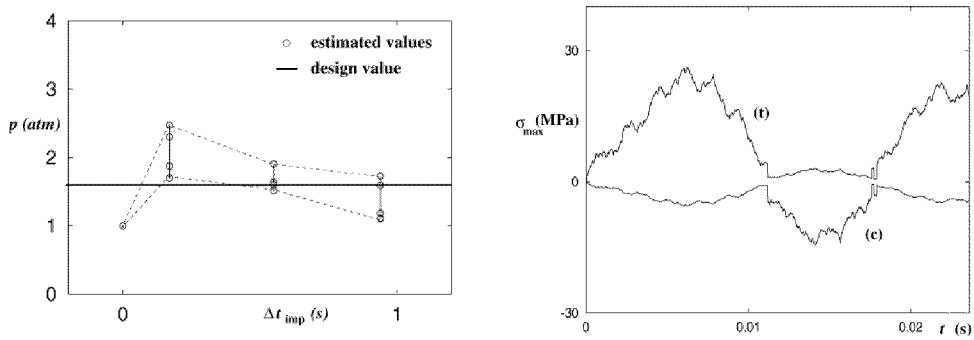

Figure 10. Left: estimated pressure evolution along beam b_1. Right: evolution of the maximum tension (t) and compression (c) stresses along beam b_2 by assuming a Dirac's delta load. All the quantities are given in full scale (D = 18 m).

The evolution of the loads on the second beam b_2 is roughly characterized by (i) an acoustic phase, (ii) a blunt-impact phase and (iii) a wedge-impact phase. The pressures associated with the initial phase are high but too localized in time and space to give any problem for the structure, *cf.* Greco *et al.* (2001b). The time duration of the second impact phase is larger than the first one, and of the same order of magnitude as the highest natural dry period of the beam, thus the elastic response of the beam could be relevant and should be further investigated. The region of the beam loaded during this blunt-impact phase is small relative to the beam length. Therefore, the evolution of beam stresses can be estimated by considering the beam subjected to a spatial Dirac-delta load, $f(t)\delta(x - x_{imp})$, located at the initial impact position. The amplitude $f(t)$ can be

estimated as the vertical force on a rigid circle penetrating a flat free surface, Faltinsen (1990), and expressed as $\rho C_s(t) r V^2$. The time dependent coefficient $C_s(t)$ has been derived experimentally by Campbell and Weynberg (1980) and is represented by the formula $C_s = 5.15/(1+8.5h/r)+0.275h/r$. Here, $h = Vt$ is the instantaneous submergence of the circle and is equal to the radius r when half-circle penetrated the free surface. From this analysis, right plot of Fig. 10, the resulting maximum stresses on the beam are safely below the yield stress (about 220 MPa). The last wedge-impact phase is more complicated and would require a more direct analysis, investigating also the possible excitation of hydroelastic effects.

Dam-break stage On a longer time scale, the observed water shipping resembles a dam-break type phenomenon. In our experiments, during this stage, the loading is mostly determined by the 'hydrostatic' pressure, since ship motions have been restrained. In reality, additional contributions are due to three-dimensional effects and deck accelerations. This phase is not expected to be dangerous for the deck structure although, depending on the amount of shipped water, it can be relevant for the dynamic behavior of the ship. This issue is not addressed here.

Deck-house impact The water front approaching the vertical superstructure resembles a thin half-wedge, and, at the beginning of the impact with the wall, only small amount of the fluid sharply deviated upwards by the obstacle is affected by the phenomenon. A jet originates vertically upwards, and spray formation is observed. Though without the modeling of the initial plunging phase, the BEM method captures well both the flow evolution on the deck and the water run-up along the vertical wall, as shown in Fig. 11 where the red lines represent numerical results. On this ground, the initial plunging phase appears not relevant for the gross features of the deck flow, as well as for impact loading on the superstructure.

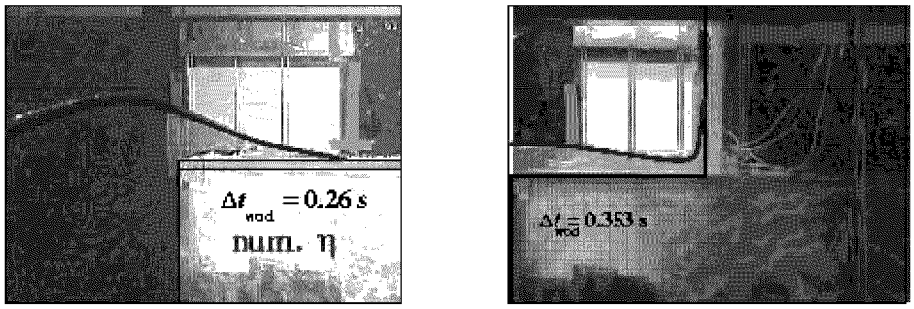

Figure 11. Left: dam break-type flow after the initial impact. Right: impact of the shipped water against the vertical wall of the deck house. The red lines are the present numerical simulations.

The pressure evolutions on the wall, measured at 0.012 m and at 0.032 m above the deck (model scale), are reported in the left and right plots of Fig. 12, respectively. Along the horizontal axis, t = 0 s corresponds to the time instant when the numerical pressure (thick line in each plot) at the lowest gauge location attains a non-zero value. Two test results are shown for each pressure gauge (full and empty symbols), showing a not-perfect repeatability and suggesting more careful measurements of local loads.

The experimental data show two pressure peaks of the same order of magnitude. The first peak is associated with the initial water impact against the superstructure. By combining the pressure measurements with the video images, we found that the second pressure peak is related to the backward water overturning, shown in Fig. 6, and appears equally important for the structural safety as the initial impact load.

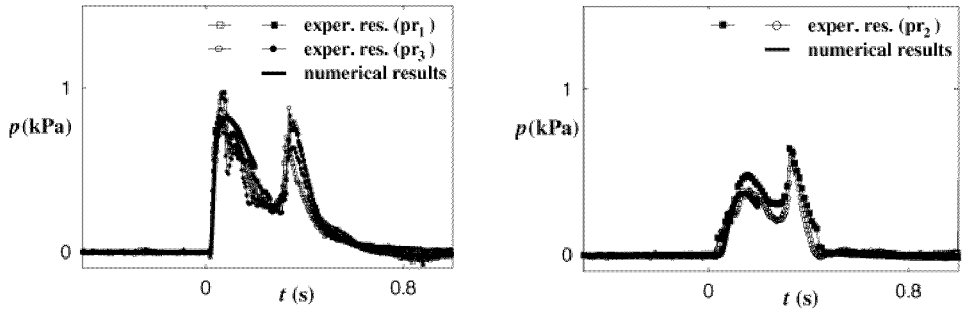

Figure 12. Pressure evolution measured on the vertical wall under impacting conditions, at 0.012 m and 0.032 m above the deck (left and right plots, respectively). Two test results are given for each gauge location. The solid lines give the numerical results, before breaking occurs and computations stopped.

The numerical prediction is rather satisfactory and recovers correctly the first pressure peak. Though the computations have been stopped as soon as the water flux entering the deck attains a zero value, the second pressure peak would not be captured anyway numerically because the boundary element method cannot handle free-surface breaking. In this respect, Level Set, Colicchio *et al.* (2002), SPH, Tulin and Landrini (2000), and VOF techniques, Greco *et al.* (2002b), have been recently proposed to handle the post-breaking evolution but they require further development and validation for extensive and practical use in this context.

Simplified tools for loading estimates

From a pre-design perspective, it is very important to develop simplified tools to quantify green-water loads. Here, we discuss a few of them by using the dam-break problem as a test case. In this framework, the BEM method has been adopted to provide reference data.

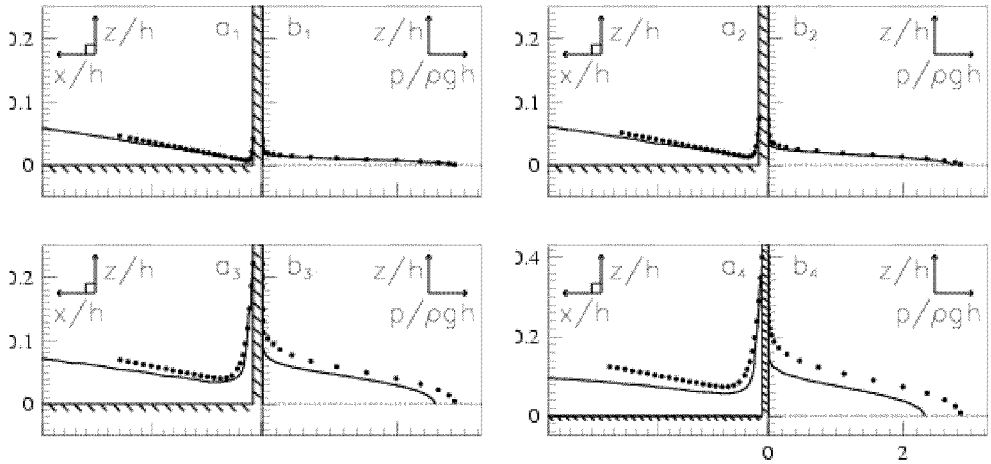

Figure 13. Free-surface profiles (a1-a4) and pressure distributions (b1-b4) during the initial stage of the impact against the vertical wall. Solid lines: present numerical simulations; •: similarity solution from Zhang *et al.* (1996). The plots are progressively enumerated as the time increases. $\Delta\tau_{imp} = \tau - \tau_{imp}$ = 0.0138, 0.0243, 0.0738, 0 .1338. τ_{imp} is the initial non-dimensional impact time.

During the initial phase of the impact, the gravity plays a minor role and the phenomenon is governed by the local-flow accelerations. Hence, the gravity-less similarity solution of a fluid wedge hitting a rigid wall, Zhang et al. (1996), describes correctly the flow field and can be used to evaluate the pressure evolution along the structure. Figure 13 shows the actual comparison between the similarity and the *exact* solution: as it can be expected, the two results start to diverge as time increases, with the approximate method over-predicting the pressure along the wall.

Within this simplified analysis, the parameters defining the impact conditions are represented by (i) the velocity V and (ii) the slope β of the water front. By using the similarity solution, Greco (2001b) has shown that $d\left(p_{\max}/\rho V^2\right)/d\beta$ is large only for β larger than, say, 60 degrees and is small for β smaller than about 40 degrees. Therefore, for small enough front slopes, the impact velocity V is the most important factor influencing the maximum pressure $p_{\max}$.

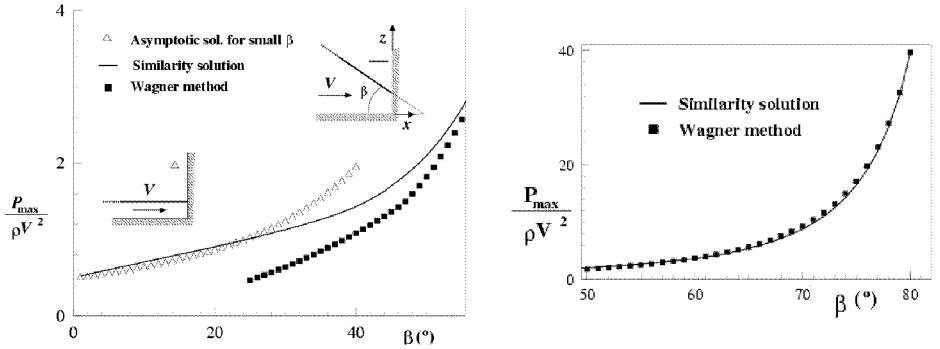

Figure 14. Maximum pressure along the wall. Left plot: the asymptotic solution for small water-front slopes β is compared with the similarity and the Wagner solutions. Right plot: for larger β, only the Wagner and the similarity solutions are shown. V: impact velocity, β: angle of the (half) wedge.

On this ground, the maximum pressure can be evaluated by even simpler methods. Figure 14 gives $p_{\max}$ onto the wall associated with the initial impact by using two different approximations valid for small and large values of the water front slope β, respectively. The first one is given in Faltinsen *et al.* (2002a), while the latter is a Wagner-type solution, Wagner (1932). The former appears suitable for $\beta \le 30^\circ$, while the latter is efficient for $45^\circ \le \beta \le 90^\circ$.

Hydroelastic effects

During the most impulsive stages, if the loading time is comparable with the structural natural wet period, hydroelastic effects are excited, and for a correct structural design the hydroelastic effects should be assessed. The influence of hydroelasticity during the water impact with the vertical wall has been investigated in Greco *et al.* (2001a) by using the dam-break problem to model the water flow along the deck and by modeling the wall structure as an Euler beam, simply supported at the ends. The structural properties are chosen by using data from typical steel stiffeners of the deck house of an actual FPSO (see sketch Fig. 15). The fluid-structure interaction is studied by coupling the nonlinear potential-flow model with the linearized beam dynamics.

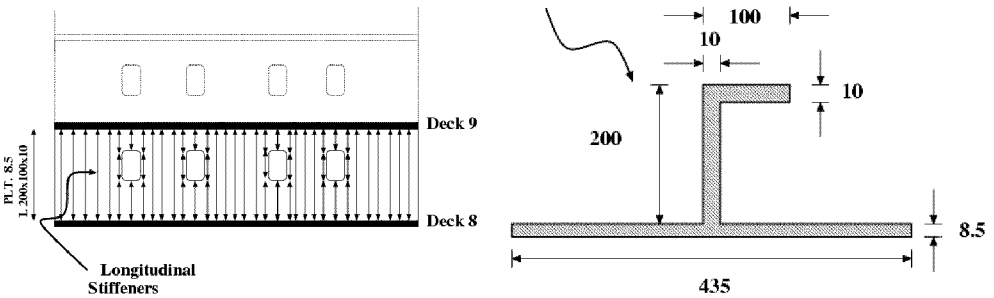

Figure 15. Example of stiffeners of a deck house (front view on the left) and cross-section of equivalent beam (on the right). Lengths are in millimeters.

The results of this analysis are summarized in Fig. 16, through the free-surface evolution during the water run-up along the structure (left) and of the maximum stresses (right) on the wall, always occurring at the lower edge of the beam. The hydroelastic results are compared with the solution obtained by assuming the structure perfectly rigid in the hydrodynamic solution and by evaluating *a posteriori* the structural deformation in a quasi-steady fashion. It is found that the free-surface configurations agree well and the magnitude of the hydroelastic stresses weakly

oscillates around a mean value slightly different than the quasi-steady solution. These observations document the limited role of hydroelasticity during the water impact with the superstructure, at least for the case here considered.

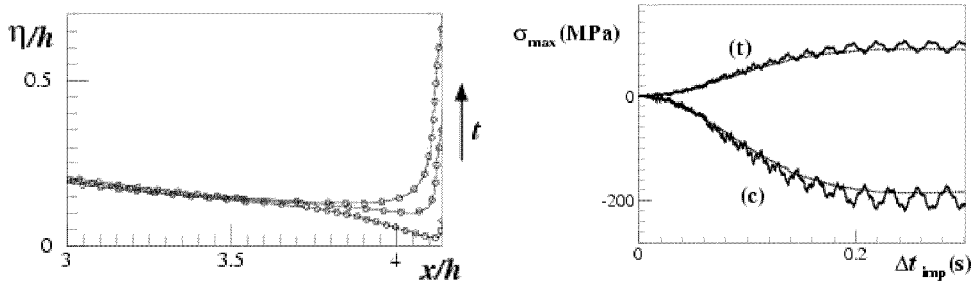

Figure 16. Impact of water with a vertical wall, the incident wave is generated by the break of a dam with initial height of the water reservoir h = 10 m. Left: free surface for three different instants after the impact for the case with rigid wall (solid lines) and hydroelastic solution (o). Right: Maximum tension (t) and compression (c) stresses as a function of time as obtained by the quasi-steady analysis (dashed lines) and by the hydroelastic analysis (solid lines).

Conclusions

The shipping of green water on a FPSO ship in head-sea has been studied by experimental and numerical means. The main stages of the flow-field evolution have been highlighted and the related loading regimes have been addressed.

It is shown that water shipping starts always with the fluid front plunging onto the deck and entrapping air in cavities of complex shape and evolution. A simplified analysis of two-dimensional experimental data shows that this air-cushion stage can lead to high pressure (very localized in space and time), and therefore to possible structural damages.

After the cavity disintegration, the following dam break-like evolution is grossly unaffected by the presence of the air bubbles dispersed within the main bulk of water. Numerical simulations, where the presence of the air-phase has been neglected, reproduce well the overall flow scenario and can be used to compute the initial conditions to study the impact against deck structures. In this context, shallow-water models may be useful although the need of boundary data may pose severe limitations to their actual applicability, see the discussion in Greco *et al.* (2000c). This stage is probably more relevant to the dynamics of the vessel rather than to the strength of the deck.

The impact against vertical deck structures is finally addressed. Although the impact loads are of main importance, laboratory measurements have shown that pressure peaks arising during the gravity driven evolution can be of the same magnitude and, therefore, of concern for design purposes.

In this framework, the potential-flow modeling has been proved reliable to simulate the flow and to predict the hydrodynamic loads at least up to breaking and fragmentation of the free surface occurs. Within this regime, even more simplified tools have been proposed which can be easily used for design and certification purposes. In the breaking regime, new strategies of numerical simulations are under development, *e.g.* Greco *et al.* (2002b).

INSEAN research activity has been supported by the Italian *Ministero per le Infrastrutture e i Trasporti* through INSEAN Research Program 2000-02.

References

Campbell I. M. C., Weynberg P. A. (1980). *Measurement of parameters affecting slamming. Final report*, Technology Reports Centre No. OT-R-8042, 440, Southampton University: Wolfson unit for marine technology.

Colicchio G., Colagrossi A., Greco M., Landrini M. (2002). *Free-surface Flow After a Dam break: A Comparative Study.* Ship Tech. Res. 49/3.

Ersdal G., Kvitrud A. (2000). *Green water on Norwegian production ships.* In 10th Int. Conf. Offshore and Polar Engng, ISOPE'2000, Seattle.

Faltinsen O. M. (1990). *Sea loads on ships and offshore structures*, Cambridge University Press, Cambridge, England.

Greco M., Faltinsen O.M., Landrini M. (2000a). *An investigation of water on deck phenomena.* In Proc. 15th Int. Workshop on Water Waves and Floating Bodies, 55-58, Eds. T. Miloh and G. Zilman, Caesarea, Israel.

Greco M., Faltinsen O.M., Landrini M. (2000b). *Basic studies of water on deck.* In Proc. 23rd Symp. on Naval Hydrod., Val de Reuil, France. National Academy Press, Washington DC.

Greco M., Faltinsen O.M., Landrini M. (2000c). *A parametric study of water on deck phenomena.* In Proc. NAV 2000, Int. Conf. on Ship and Shipping Research, Venice, Italy.

Greco M., Faltinsen O.M., Landrini M. (2001a). *Green Water Loading on a Deck Structure.* In Proc. 16th Int. Workshop on Water Waves and Floating Bodies, Hiroshima, Japan.

Greco M. (2001b). *A Two-dimensional Study of Green-Water Loading.* Ph. D. Thesis, Dept. Marine Hydrodynamics, NTNU, Norway.

Faltinsen O.M., Greco M., Landrini M. (2002a). *Green-water loading on a FPSO.* J. Off. Mech Arc. Engng. (ASME), 124.

Greco M., Faltinsen O.M., Landrini M. (2002b). *Water Shipping on a Vessel in Head Waves.* In Proc. of 24th Symp. on Naval Hydrodynamics, Kyushu (Japan).

Rapp R.J., Melville W.K. (1990). *Laboratory Measurement of Deep-Water Breaking Waves.* Phil. Trans. of the Royal Soc. of London, Series A, 331, pp.735-800.

Salvesen N., Tuck E.O., Faltinsen O.M. (1970). *Ships motions and Sea Loads.* SNAME Trans. 78. 250-287.

Tulin M.P., Landrini M. (2000). *Breaking waves in the ocean and around ships.* In Proc. 23rd Symp. on Naval Hydrodynamics, Val de Reuil, France. National Academy Press, Washington DC.

Wagner H. (1932). *Uber stoss- und gleitvorgange an der oberflache von flussigkeiten.* ZAMM, 12, No. 4, pp. 192-235.

Zhang S., Yue D. K. P., Tanizawa K. (1996). *Simulation of plunging wave impact on a vertical wall.* J. Fluid Mech., 327, pp. 221-254.

Zhao R., Faltinsen O.M., Aarnes J. (1997). *Water entry of arbitrary two-dimensional sections with and without flow separation.* In Proc. of 21st Symp. on Naval Hydrod., National Academy Press, Trondheim, Norway. Val de Reuil, France. National Academy Press, Washington DC.